Supplementary Information (SI) for Inorganic Chemistry Frontiers.

Supporting Information

Size Matters: Altering the Metal-Surface Coordination in Micropores via Structural Confinement Effects

Scott A. Southern[a], Austin Thompson[b], Aaron D. Sadow[a,b], and Frédéric A. Perras[*a,b]

a. Chemical and Biological Sciences Division, Ames National Laboratory, Ames, IA 50011 (USA)
b. Department of Chemistry, Iowa State University, Ames, IA 50011 (USA)

Correspondence: fperras@ameslab.gov

Table of Contents

1. Simulation of PARS Spectra with Intermediate Dynamics

1.1. Typical Input Parameters

We employed a fitting procedure using a homebuilt C/C++ program we developed to simulate dipolar coupling doublets pairs of nuclei experiencing dynamic jump motions. Powder averaging was accomplished using 2000 orientations generated using the REPULSION scheme.[1] Each experimental doublet, representing C_2 jump dynamics, was simulated using a ^{13}C-^{1}H dipolar coupling constant of 23.2 kHz, and an exchange constant, k, calculated using the Eyring equation for the specific sample temperature and activation energy, ^{E_A}. The modeling approach is described in greater detail in section 1.2.

1.2. Simulation of PARS Spectra with Intermediate Dynamics

PARS spectra containing dynamics of intermediate timescale were simulated assuming a 2-site exchange model that can be treated analytically.[2] We assume a static orientation of the 2-site system where the dipolar coupling constant is scaled by the recoupling sequence's (wR18$_2^5$) scaling factor (κ=0.223) and the exchange occurs at a rate of k. The exchange matrix is given by.

$$L = \begin{bmatrix} i\kappa\omega_{D,A} - k & k \\ k & i\kappa\omega_{D,B} - k \end{bmatrix}$$

where $^{\omega_{D,A}}$ and $^{\omega_{D,B}}$ are the dipolar frequencies associated with both orientations.

$$\omega_{D,A} = 2\pi D\left(3cos^2\beta - 1\right)$$

The NMR signals evolves as exp(**L**) which produces two Lorentzians:

$$l_1 = e^{-kt}e^{i\bar{\omega}t}e^{-\frac{t}{2}\sqrt{4k^2-\omega_\Delta^2}}$$
$$l_2 = e^{-kt}e^{i\bar{\omega}t}e^{\frac{t}{2}\sqrt{4k^2-\omega_\Delta^2}}$$

where,

$$\bar{\omega} = (\kappa\omega_{D,A} + \kappa\omega_{D,B})/2$$
$$\omega_\Delta = \kappa\omega_{D,A} - \kappa\omega_{D,B}$$

These Lorentzians have linewidths characterized by R_2 values of:

$$R_2 = \begin{cases} k & \omega_\Delta^2 \geq 4k^2 \\ k - \frac{1}{2}\sqrt{4k^2-\omega_\Delta^2} & \omega_\Delta^2 < 4k^2 \end{cases}$$

To simulate *R*-symmetry lineshapes, we then adopt the appropriate orientational dependence for the recoupled lineshape

$$f \propto \kappa D\left(3sin^2\beta + \eta cos2\alpha(1+cos\beta)^2/2\right)$$

and introduce two conditions, namely, whether the dynamics are faster or slower than the resonance frequency differed in that powder orientation.

$$e^{i\langle f_X\rangle t}e^{R_2 t} = \begin{cases} e^{if_X t}e^{kt} & \omega_\Delta^2 \geq 4k^2 \\ e^{i\langle f\rangle t}e^{\left(k+\frac{1}{2}\sqrt{4k^2-\omega_\Delta^2}\right)t} & \omega_\Delta^2 < 4k^2 \end{cases}$$

This is an approximation of the expected lineshape but enables for the accurate simulation of coalescence in R-symmetry-based dipolar recoupling experiments. Powder averaging over Euler angles is then performed and a Fourier transform is applied to convert the time dependence described above into the recoupled lineshapes.

2. Supplementary Synthetic Methods

General. Dry solvents were obtained from an Innovative Technologies solvent purification system and stored over molecular sieves under inert gas. Benzene-d_6 was dried by stirring over NaK followed by vacuum transfer. Aniline was purchased from Sigma-Aldrich and was used as received. Potassium hydride (Sigma-Aldrich) suspended in mineral oil was washed with dry pentane, dried in vacuo, and stored in an N_2-filled glovebox. Anhydrous $LaCl_3$, $ScCl_3$, and YCl_3 were obtained from Strem Chemicals and used as received. Sc{(N^{i}Pr)$_2$CH}$_3$ was obtained from Strem and sublimed before use. Triethyl orthoformate (formyl-^{13}C, 99%) and aniline ($^{13}C_6$, 99%) were obtained from Cambridge Isotope Laboratories and used as received. Solution-state NMR spectra were acquired on either a Bruker AVIII-600 or a Bruker NEO-400 spectrometer. Spectra were calibrated with reference to the residual ^{1}H signal in the deuterated solvent. Fourier transform infrared spectroscopy (FTIR) and diffuse reflectance infrared Fourier transform spectroscopy (DRIFTS) were acquired using a Bruker Vertex 80 spectrometer. Silica supports (Sigma-Aldrich) were calcined at 500 °C under air for 12 h (ramp rate 2 °C/min), partially dehydroxylated under dynamic vacuum at 550 °C for 12 h (ramp rate 2 °C/min) and stored in an N_2-filled glovebox. The silanol content in the silica materials was measured by NMR titration using the protonation of Bn_2Mg to form toluene in benzene-d_6 with tetrakis(trimethylsilyl)silane (TMSS) as an internal standard of known concentration.

Metal loadings were determined by solution-state NMR. Briefly, amidinate complexes were first dissolved in a Youngs tap fitted NMR tube using benzene-d_6 with TMSS as an internal standard. Using this standard, the millimoles (mmol) of the complex was determined by ^{1}H NMR integration. A known amount of silica (based on silanol concentration, 0.9 equiv.) was then added to the NMR tube and allowed to mix for 24 h. Following this reaction, the residual concentration of the free metal complex was again quantified to determine the mmol of the complex that was consumed.

Physisorption isotherms were measured in a Micromeritics Tristar surface area and porosity analyzer. The surface area was calculated by the Brunauer-Emmett-Teller (BET) method.

Yttrium tris[*N,N′*-bis(phenyl-$^{13}C_6$)formamidate-$^{13}C_{13}$] (Y{κ^2-(NPh)$_2$CH-$^{13}C_{13}$}$_3$). YCl_3 (0.045 g, 0.230 mmol, 1 equiv.) was suspended in anhydrous THF (8 mL) and stirred vigorously. A THF solution of K[(NPh)$_2$CH-$^{13}C_{13}$] (0.164 g, 0.690 mmol, 3 equiv.) was added in a dropwise fashion to the stirring suspension. The reaction mixture became increasingly turbid as it was stirred for 12 h. The solution was filtered through a 0.45 μm glass fiber filter, and the solvent removed *in vacuo*. The residue was lyophilized by dissolving in benzene (5 mL), freezing the solution, and subliming the benzene *in vacuo* to yield Y{κ^2-(NPh)$_2$CH-$^{13}C_{13}$}$_3$ (0.146 g, 92.5%) as a pale-yellow solid, which was used without further purification. ^{1}H NMR (400 MHz, benzene-d_6): δ 7.82 (d, $^1J_{CH}$ = 173.6 Hz, 3 H, formyl ^{13}CH), 7.10 (vt, $^1J_{CH}$ = 155 Hz (satellite), $^3J_{HH}$ = 8 Hz, 12 H, *meta*-C_6H_5), 6.9 (m, 18 H, *ortho*/*para*-C_6H_5). ^{13}C{^{1}H} NMR (100.6 MHz, benzene-d_6): δ 149.5 (br s, formyl ^{13}CH), 146.1 (t, $^1J_{CC}$ = 61.6 Hz, *ipso*-C_6H_5), 129.5 (td, $^1J_{CC}$ = 56.9, $^3J_{CC}$ = 7.1 Hz, *meta*-C_6H_5), 123.3 (td, $^1J_{CC}$ = 56.1 Hz, $^3J_{CC}$ = 9.5 Hz, *para*-C_6H_5), 119.6 (vt, $^1J_{CC}$ = 58.9 Hz, *ortho*-C_6H_5).

Lanthanum tris[*N,N′*-bis(phenyl-$^{13}C_6$)formamidate-$^{13}C_{13}$] (La{κ^2-(NPh)$_2$CH-$^{13}C_{13}$}$_3$). La{κ^2-(NPh)$_2$CH-$^{13}C_{13}$}$_3$ was prepared following the procedure described for Y{κ^2-(NPh)$_2$CH-$^{13}C_{13}$}$_3$. $LaCl_3$ (0.040 g, 0.163 mmol, 1 equiv.) and K[(NPh)$_2$CH-$^{13}C_{13}$] (0.117 g, 0.492 mmol, 3 equiv.) were combined to afford La{(NPh)$_2$CH-$^{13}C_{13}$}$_3$ (0.107 g, 89.2%) as a pale-yellow solid. ^{1}H NMR (400 MHz, benzene-d_6): δ 8.378 (d, $^1J_{CH}$ = 162.4 Hz, 3 H, formyl ^{13}C*H*), 7.21 (t, $^1J_{CH}$ = 154 Hz (satellite), $^3J_{HH}$ = 8.0 Hz, 12 H, *meta*-C_6H_5), 6.92 (m, 18 H, *ortho*/*para*-C_6H_5).^{13}C{^{1}H} NMR (100.6 MHz, benzene-d_6): δ 156.9 (s, formyl ^{13}CH), 151.3 (t, $^1J_{CC}$ = 62.3 Hz, *ipso*-C_6H_5), 129.7 (td, $^1J_{CC}$ = 57.3 Hz, $^3J_{CC}$ = 7.8 Hz, *meta*-C_6H_5), 121.5 (td, $^1J_{CC}$ = 55.8 Hz, $^3J_{CC}$ = 8.9 Hz, *para*-C_6H_5), 120.0 (t, *J* = 59.9 Hz, *ortho*-C_6H_5).

Natural Abundance. Y{κ^2-(NPh)$_2$CH}$_3$, La{κ^2-(NPh)$_2$CH}$_3$, and Sc{κ^2-(NPh)$_2$CH}$_3$, at natural abundance, were synthesized in an analogous manner to that of the enriched species.

Yttrium tris[*N,N′*-bis(phenyl)formamidate] tetrahydrofuran (Y{κ^2-(NPh)$_2$CH}$_3$)·THF. YCl_3 (0.198 g, 1.01 mmol, 1 equiv.) and K[(NPh)$_2$CH] (0.710 g, 3.03 mmol, 3 equiv.) afforded Y{κ^2-(NPh)$_2$CH}$_3$·THF as yellow solid (0.468 g, 61.8%). ^{1}H NMR (600 MHz, benzene-d_6): δ 8.88 (s, 3 H, formyl), 7.08 (t, $^3J_{HH}$ = 8.4 Hz, 12 H, *meta*-C_6H_5), 6.96 (d, $^3J_{HH}$ = 7.8 Hz, 12 H, *ortho*-C_6H_5), 6.88 (t, $^3J_{HH}$ = 7.2 Hz, 6 H, *para*-C_6H_5). ^{13}C{^{1}H} NMR (151 MHz, benzene-d_6): δ 163.9 (formyl), 149.2 (*ipso*-C_6H_5), 129.0 (*meta*-C_6H_5), 122.2 (*para*-C_6H_5), 120.2 (*ortho*-C_6H_5), 69.9 (THF), 24.7 (THF). IR (KBr, cm^{-1}): 3053 w, 3031 w, 2910, w, 2890 w, 1649 m, 1587 m, 1527 s, 1485 s, 1385 m, 1288 s, 1218 m, 1172 w, 1152 w, 1076 w, 1027 w, 988 w, 944 w, 897 w, 868 w, 831 w, 810 w, 758 s, 692 s. Anal. Calcd for $C_{43}H_{41}N_6OY$: C, 69.16; H, 5.53; N, 11.25. Found: C, 68.98; H, 5.45; N, 11.09.

Lanthanum tris[*N,N′*-bis(phenyl)formamidate] (La{κ^2-(NPh)$_2$CH}$_3$). $LaCl_3$ (0.258 g, 1.05 mmol, 1 equiv.) and K[(NPh)$_2$CH] (0.738 g, 3.15 mmol, 3 equiv.) were combined to afford La{(NPh)$_2$CH}$_3$ (0.539 g, 68.7%) as a pale-yellow solid. ^{1}H NMR (600 MHz, benzene-d_6): δ 8.62 (s, 3 H, formyl), 7.26 (t, $^3J_{HH}$ = 7.2 Hz, 12 H, *meta*-C_6H_5), 6.93 (m, 18 H, *ortho*/*para*-C_6H_5). ^{13}C{^{1}H} NMR (151 MHz, benzene-d_6): δ 160.4 (formyl), 153.6 (*ipso*-C_6H_5), 129.8 (*meta*-C_6H_5), 120.8 (*para*-C_6H_5), 120.3 (*ortho*-C_6H_5). IR (KBr, cm^{-1}): 3051 w, 3020 w, 1679 w, 1650 m, 1558 m, 1529 s, 1476 s, 1385 w, 1324 s, 1220 m, 1205 m, 1170 m, 1152 w, 1075 w, 1024 w, 986 s, 917 w, 887 w, 831 w, 804 w, 764 s, 697 s, 619 w, 594 w, 524 m. Anal. Calcd for $C_{39}H_{33}N_6La$: C, 64.64; H, 5.59; N, 11.60. Found: C, 64.51; H, 5.57; N, 11.22.

Scandium tris[*N*,*N*′-bis(phenyl)formamidate] (Sc{κ^2-(NPh)$_2$CH}$_3$). $ScCl_3$ (0.157 g, 1.04 mmol, 1 equiv.) and K[(NPh)$_2$CH] (0.731 g, 3.12 mmol, 3 equiv.) afforded Sc{κ^2-(NPh)$_2$CH}$_3$ (0.431 g, 65.7%) as a pale-yellow solid. ^{1}H NMR (600 MHz, benzene-d_6): δ 8.27 (broad singlet, 3 H, formyl), 7.08 (t, $^3J_{HH}$ = 7.8 Hz, 12 H, *meta*-C_6H_5), 6.90 (m, 18 H, *ortho*/*para*-C_6H_5). ^{13}C{^{1}H} NMR (151 MHz, benzene-d_6): δ 154.2 (br, formyl C-H), 146.4 (br, *ipso*-C_6H_5), 129.5 (*meta*-C_6H_5), 123.4 (*para*-C_6H_5), 119.8 (*ortho*-C_6H_5). IR (KBr, cm^{-1}): 3053 w, 2029 w, 2918 w, 2852 w, 1651 s, 1587 s, 1524 s, 1487 s, 1384 m, 1287 s, 1225 m, 1208 w, 1172 w, 1154 w, 1076 w, 1026 w, 999 w, 986 w, 953 w, 898 w, 806 w, 756 s, 695 s. Anal. Calcd for $C_{39}H_{36}N_6Sc$: C, 74.27; H, 5.27; N, 13.33. Found: C, 73.95; H, 5.21; N, 13.56.

3. Supplementary Tables and Figures

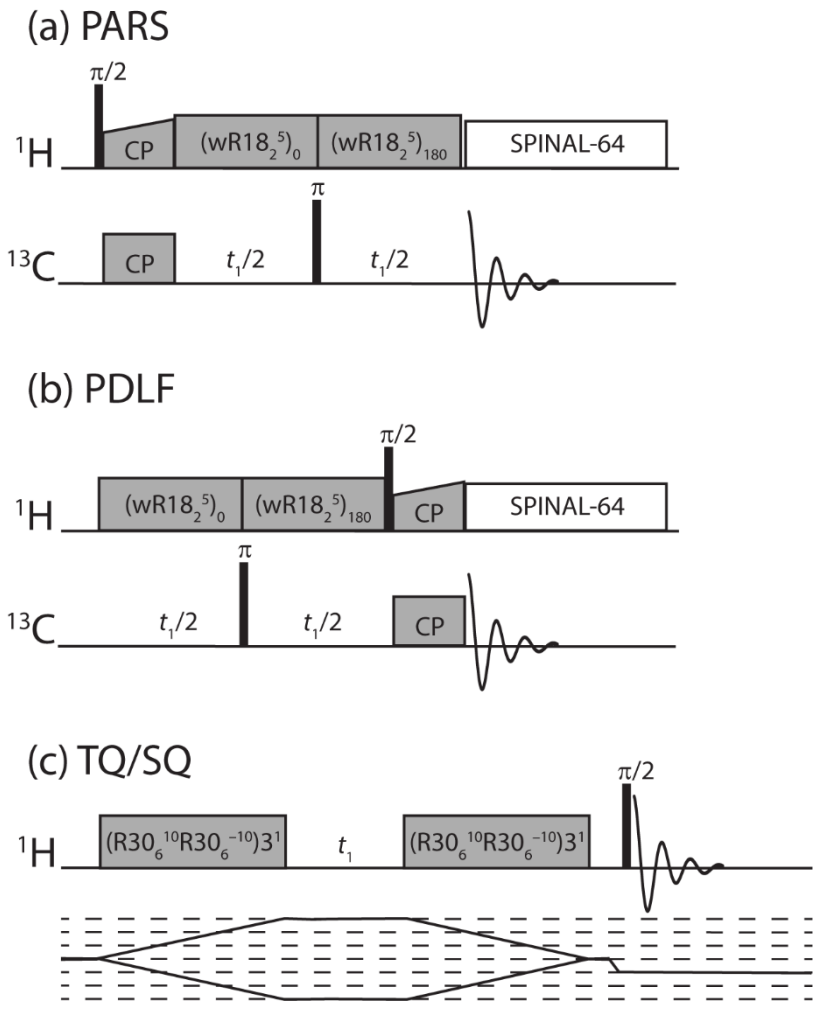

Figure S1. Specialised NMR pulse sequences used in the study: (a) PARS, (b) PDLF, and (c) TQ/SQ.

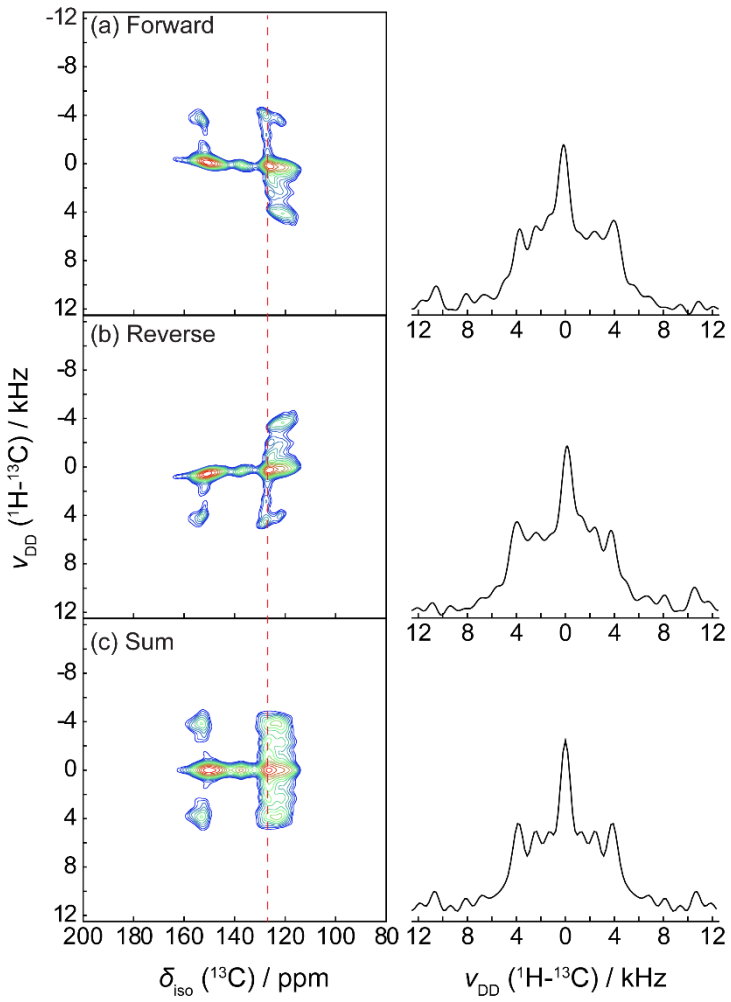

Figure S2. Representative process for obtaining cosine-transformed 2D separated local field spectra. Inverted (b) and non-inverted (a) QF-processed 2D spectra and their sum (c), which is mathematically equivalent to a pure-cosine transformation when no phase corrections are applied. PARS and PDLF data are pure cosine modulated and are best represented by cosine-transformations. The red dashed line indicates the area from which the slices shown to the right are taken.

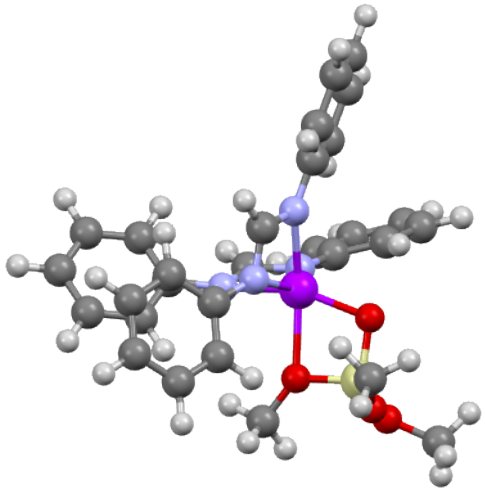

Figure S3 Geometry-optimized DFT cluster model structure of Sc{κ^2-$(NPh)_2CH$}$_2$/SiO_2

Table S1. Silanol content in partially dehydroxylated silica.

Silica	SiOH (mmol/g)	-OH nm^{-2}
Davisil, Grade 643, 150 Å	0.094 ± 0.0056	0.095
Davisil, Grade 635, 60 Å	0.62 ± 0.0092	1.44
Davisil Grade 923, 30 Å	0.41 ± 0.028	0.53
Davisil, Grade 12, 22 Å	0.097 ± 0.0065	0.094

Table S2: ^{1}H NMR determined metal loadings.[a]

Silica	Y{κ^2-(NPh)$_2$CH}$_3$	La{κ^2-(NPh)$_2$CH}$_3$	Sc{κ^2-(NPh)$_2$CH}$_3$	Sc{κ^2-(N*i*Pr)$_2$CH}$_3$
Davisil, Grade 643, 150 Å	--	--	0.062[b]	--
Davisil, Grade 635, 60 Å	0.253	0.225	0.254	0.473
Davisil, Grade 923, 30 Å	--	--	0.170	--
Davisil, Grade 12, 22 Å	--	--	0.018[b]	--

[a]mmol/g

[b]Note that these two silica materials have lower OH densities, which led to lower metal loadings, see **Table S1.**

Table S3. BET determined surface area and pore volume of the bare Davisil-type silicas and those measured after grafting Sc{κ^2-(NPh)$_2$CH}$_3$.[a]

Silica	Ungrafted Surface Area[a]	Grafted Surface Area[a]	Ungrafted Pore volume[b]	Grafted Pore Volume[b]
Davisil, Grade 643, 150 Å	599.0	488.4	0.3099	0.2583
Davisil, Grade 635, 60 Å	258.9	286.8	0.8928	0.7599
Davisil, Grade 923, 30 Å	462.1	345.4	0.3397	0.2535
Davisil, Grade 12, 22 Å	621.2	472.1	0.3017	0.2475

[a]m^2/g, [b]cm^3/g

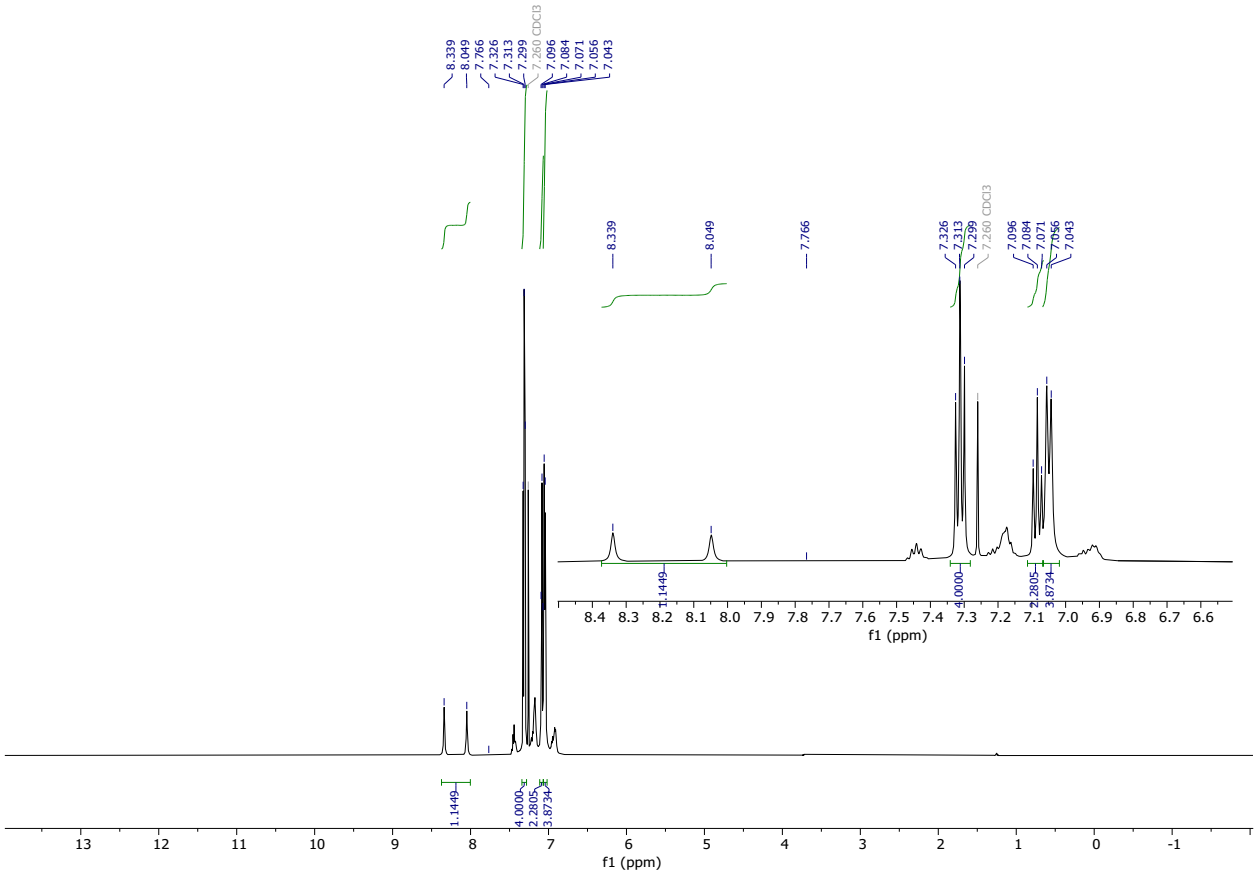

Figure S4. ^{1}H NMR spectrum of *N*,*N*′-bis(phenyl)formamidine-$^{13}C_{13}$ (chloroform-*d*).

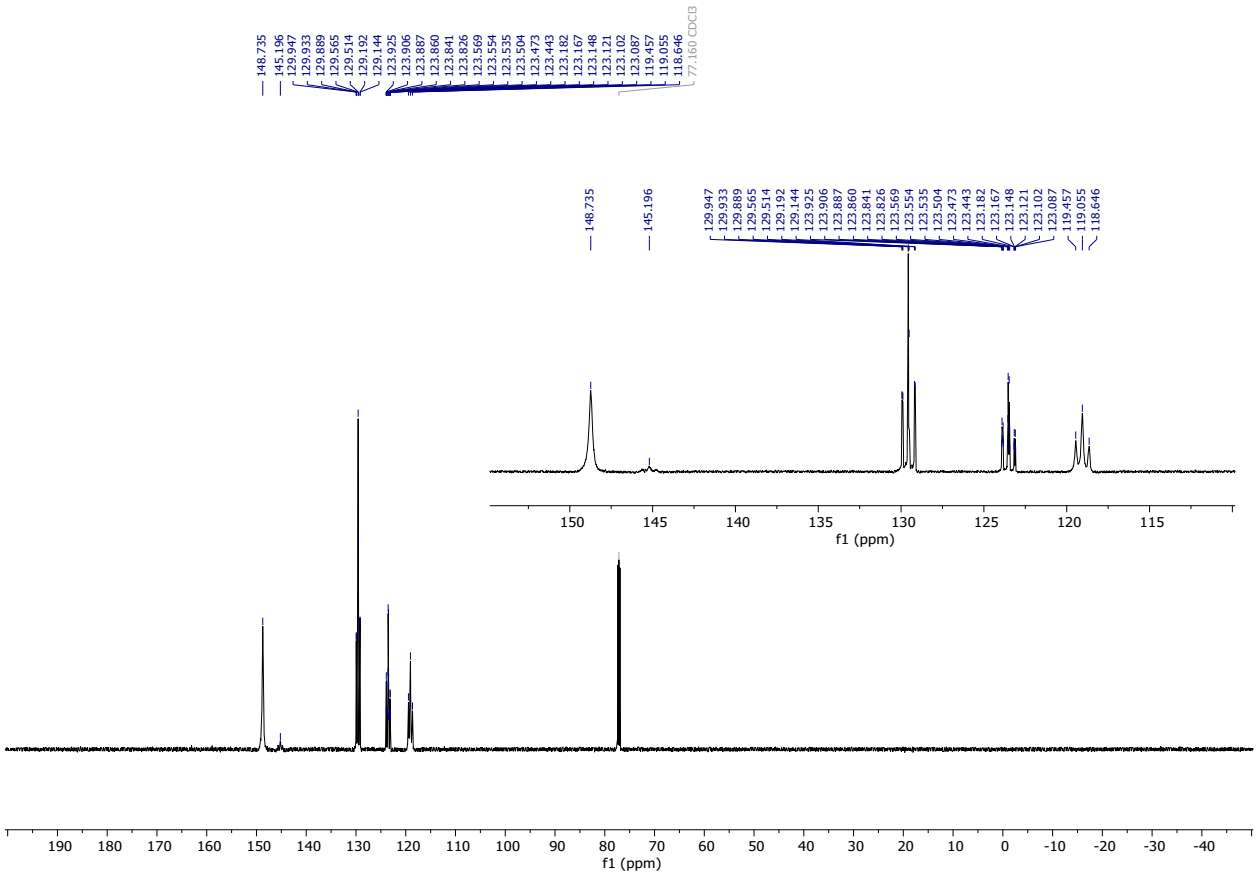

Figure S5. $^{13}C\{^{1}H\}$ NMR spectrum of *N*,*N*′-bis(phenyl)formamidine-$^{13}C_{13}$ (chloroform-*d*).

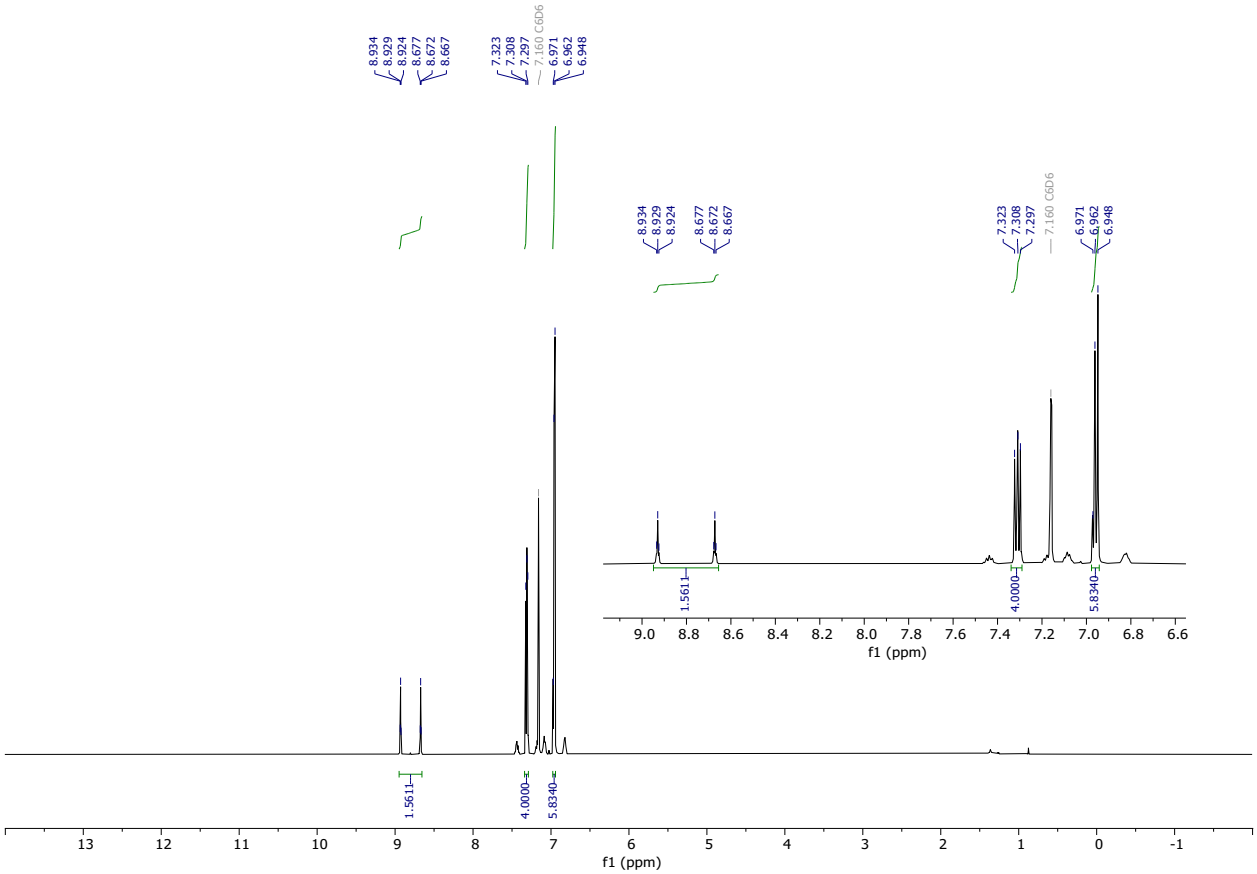

Figure S6. ^{1}H NMR spectrum of potassium *N*,*N*′-bis(phenyl)formamidate-$^{13}C_{13}$ (benzene-d_6).

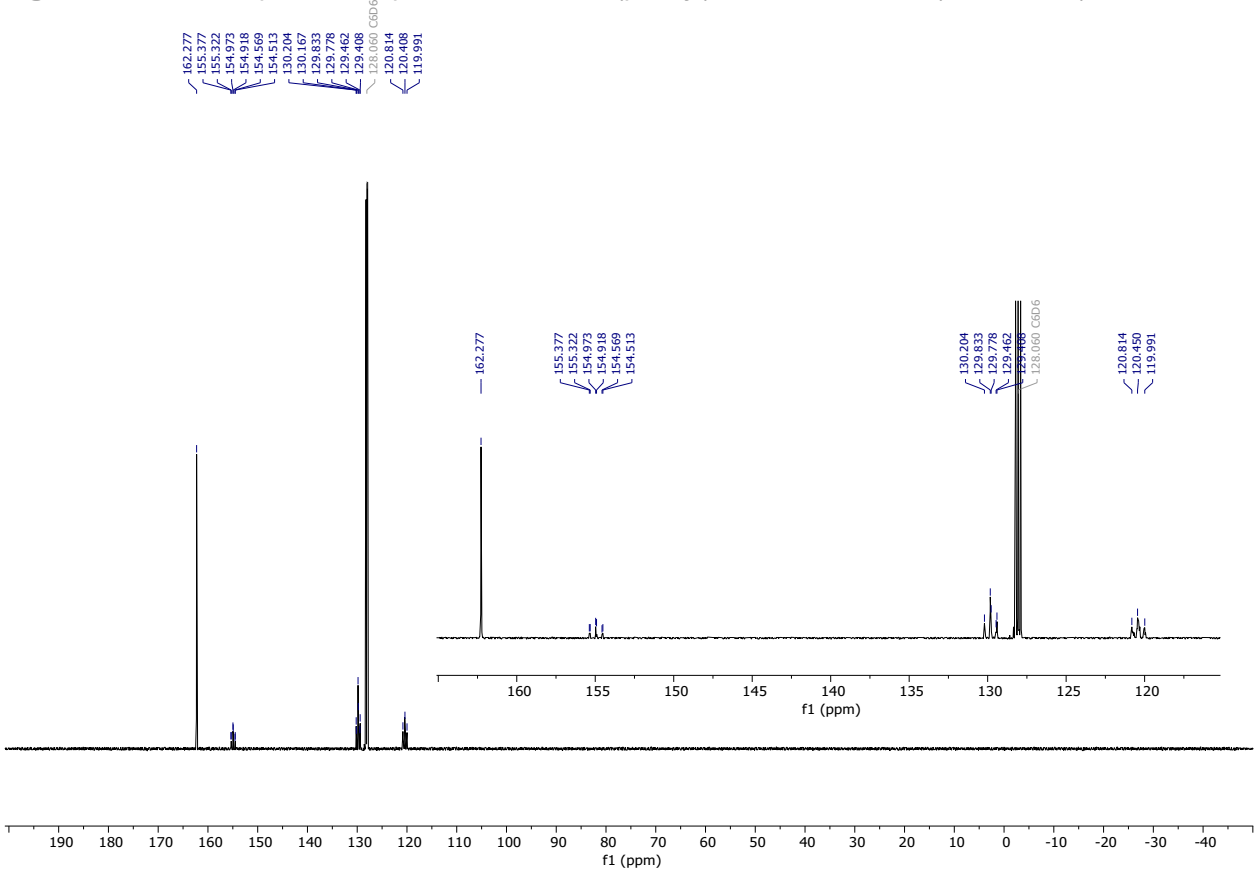

Figure S7. $^{13}C\{^{1}H\}$ NMR spectrum of potassium *N*,*N*′-bis(phenyl)formamidate-$^{13}C_{13}$ (benzene-d_6).

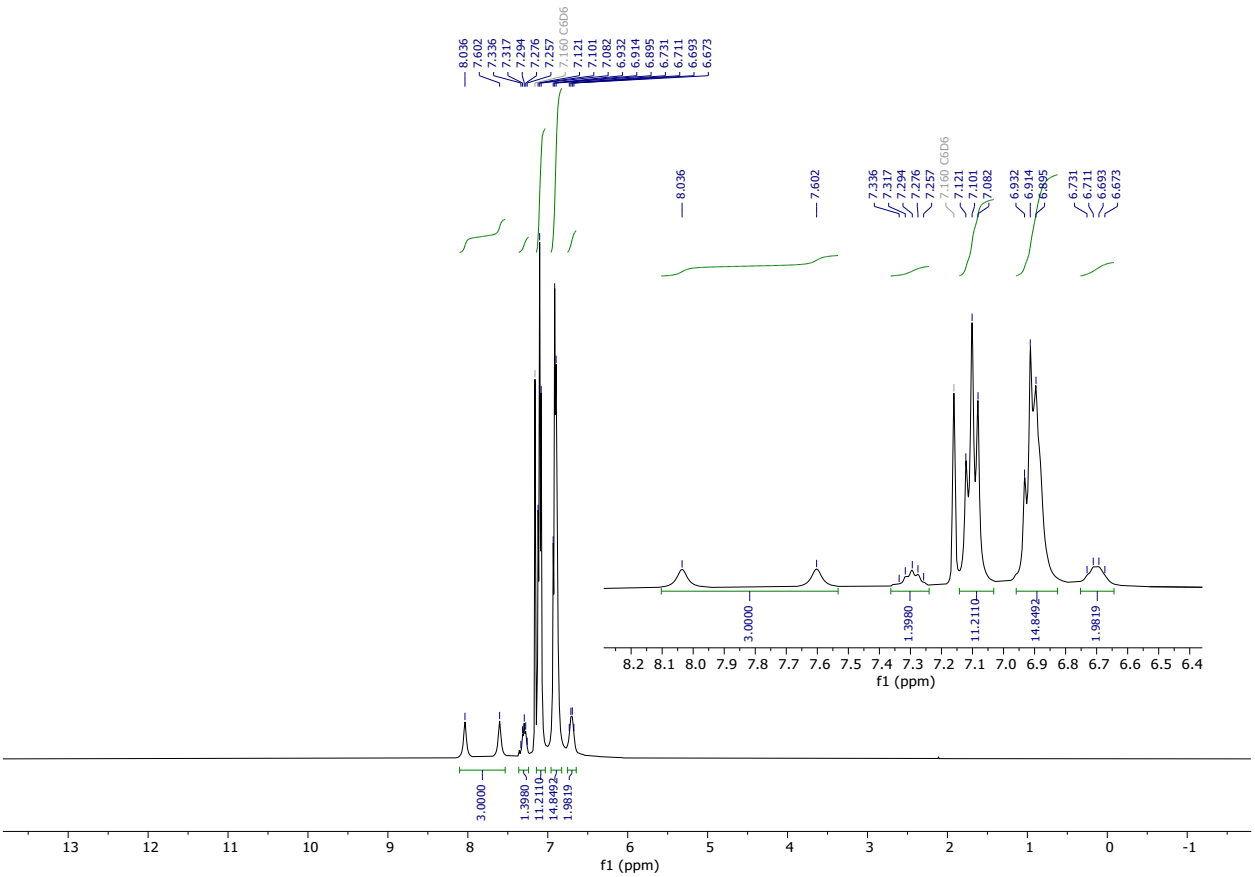

Figure S8. ^{1}H NMR spectrum of Y{κ^{2}-(NPh)$_{2}$CH-^{13}C$_{13}$}$_{3}$ in benzene-d_{6}.

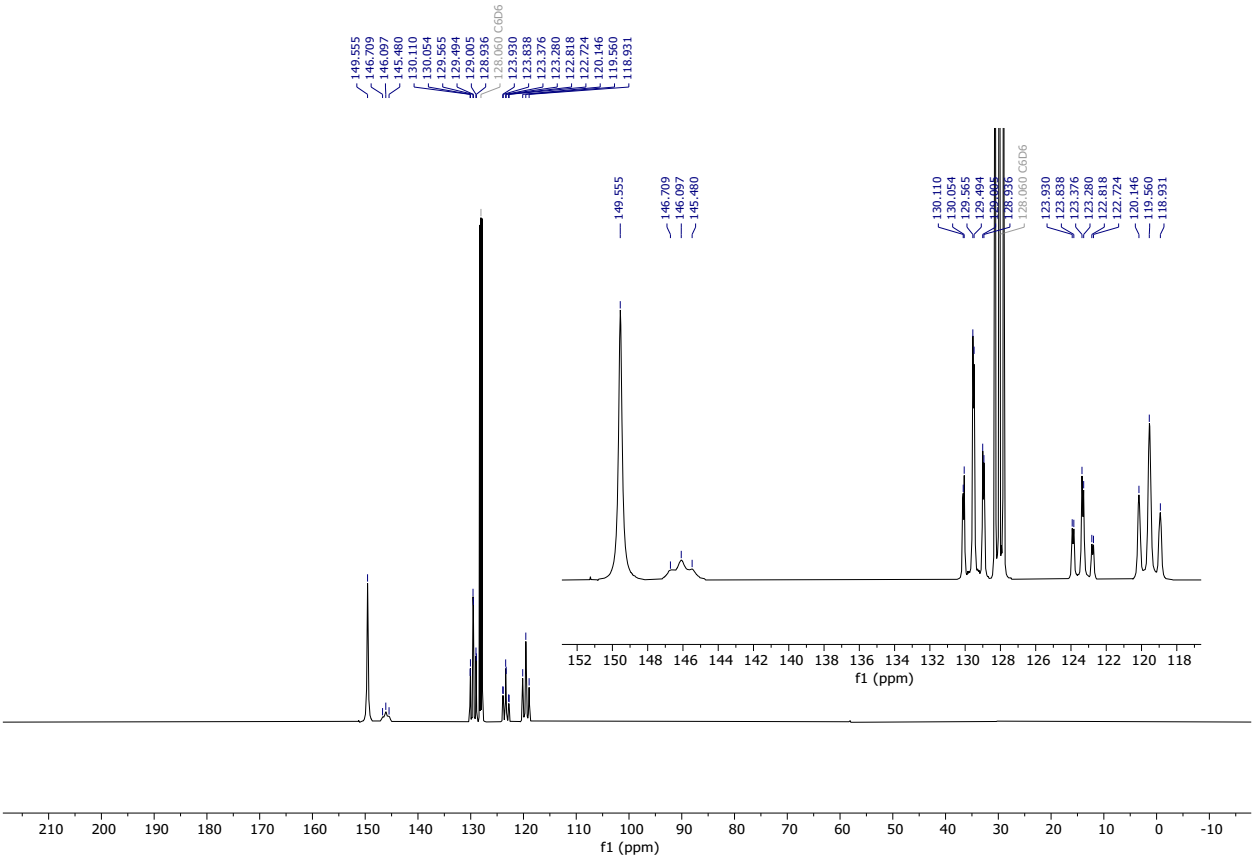

Figure S9. ^{13}C{^{1}H} NMR spectrum of Y{κ^{2}-(NPh)$_{2}$CH-^{13}C$_{13}$}$_{3}$ in benzene-d_{6}.

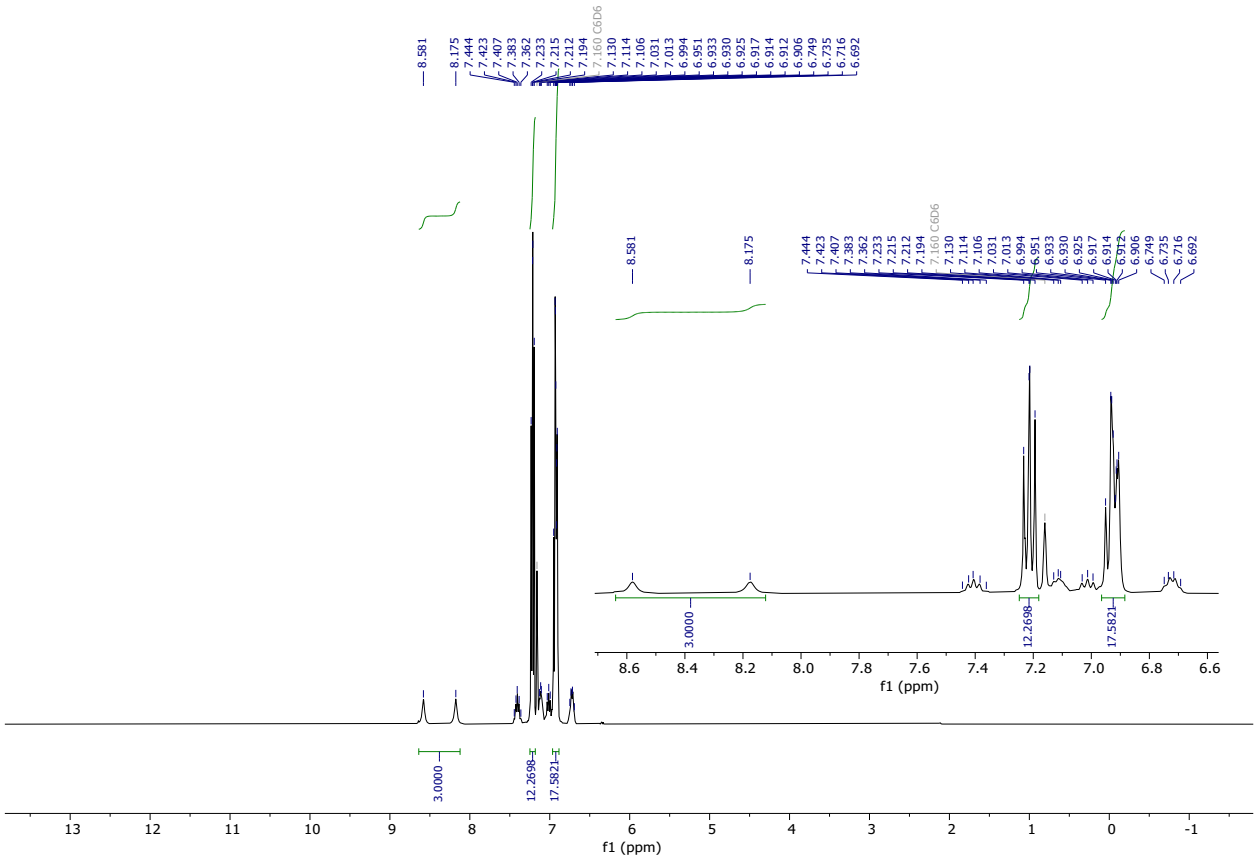

Figure S10. ^{1}H NMR spectrum of La{κ^{2}-(NPh)$_{2}$CH-^{13}C$_{13}$}$_{3}$ in benzene-d_6.

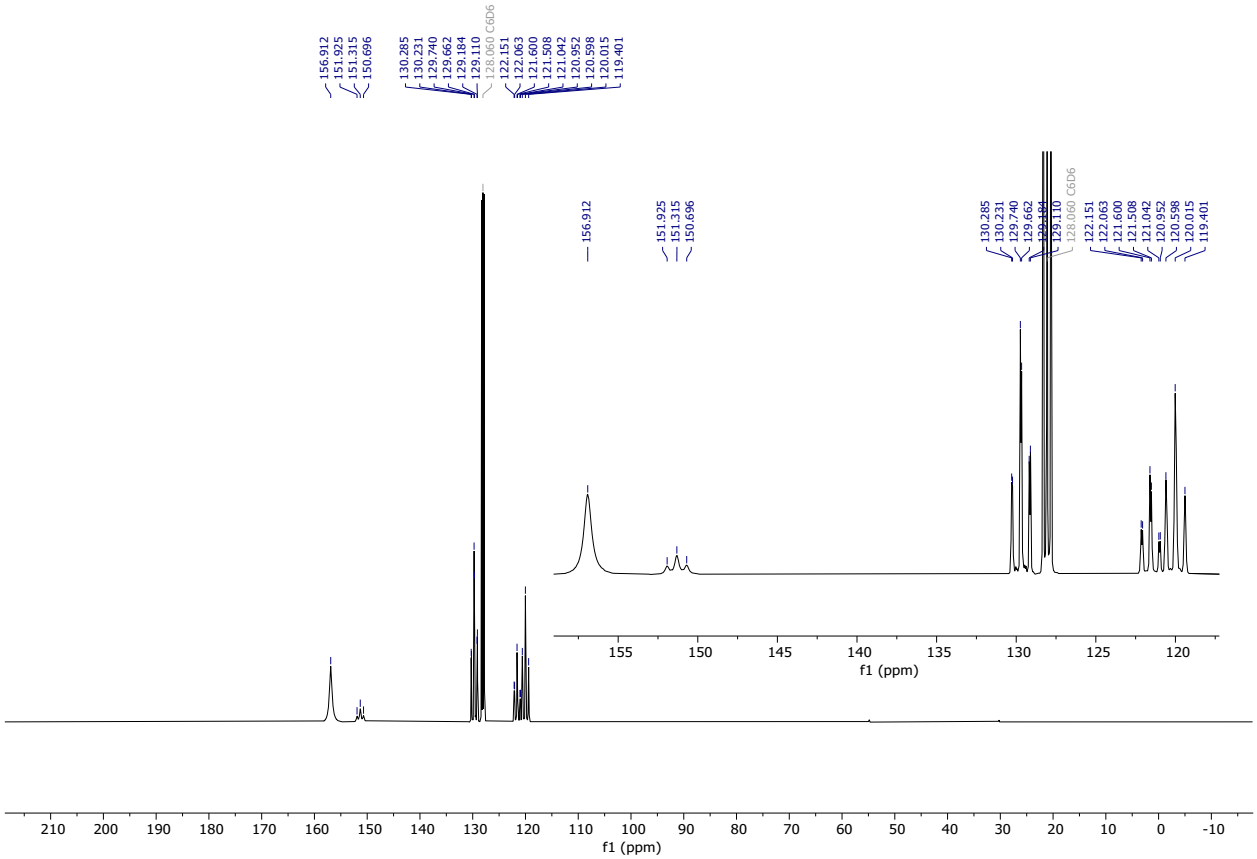

Figure S11. ^{13}C{^{1}H} NMR spectrum of La{κ^{2}-(NPh)$_{2}$CH-^{13}C$_{13}$}$_{3}$ in benzene-d_6.

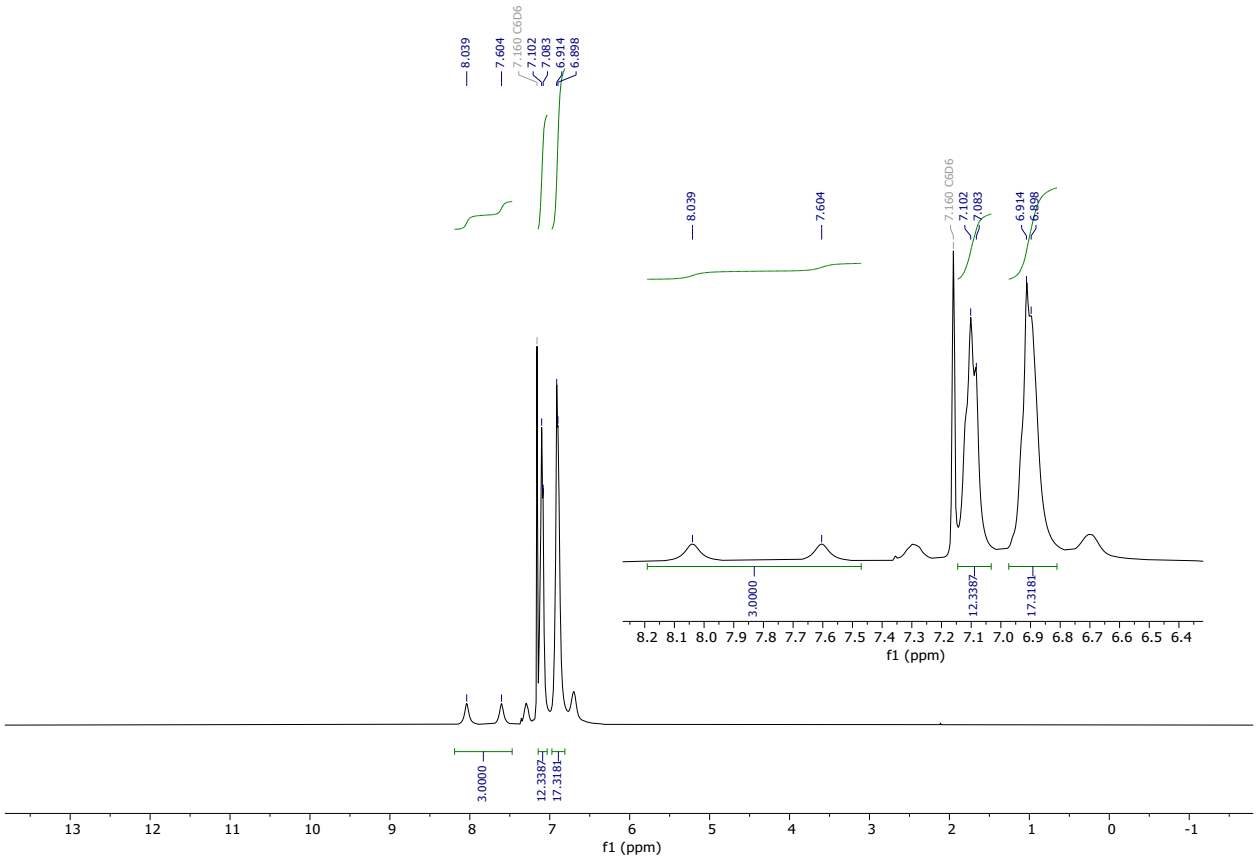

Figure S12. ^{1}H NMR spectrum of Sc{κ^{2}-(NPh)$_{2}$CH-^{13}C$_{13}$}$_{3}$ in benzene-d_{6}.

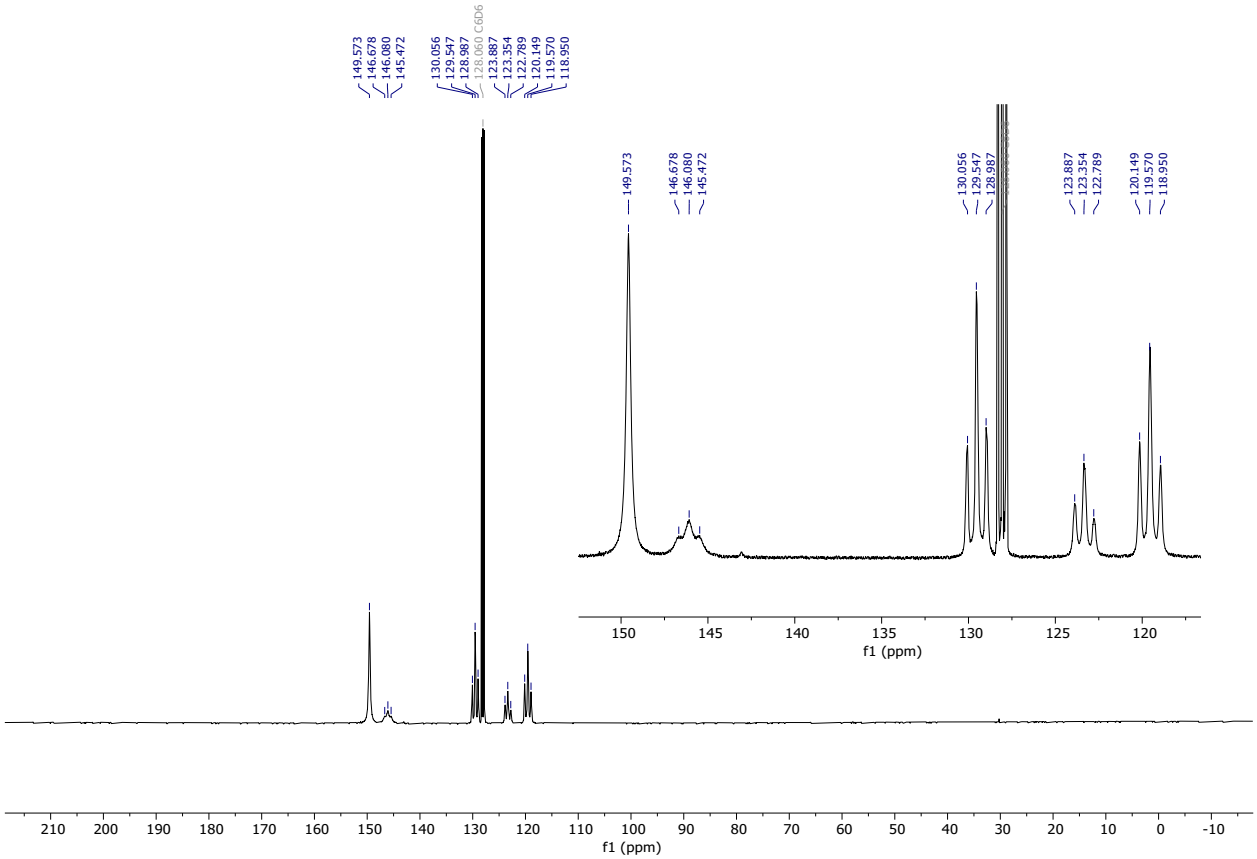

Figure S13 ^{13}C{^{1}H} NMR spectrum of Sc{κ^{2}-(NPh)$_{2}$CH-^{13}C$_{13}$}$_{3}$ in benzene-d_{6}.

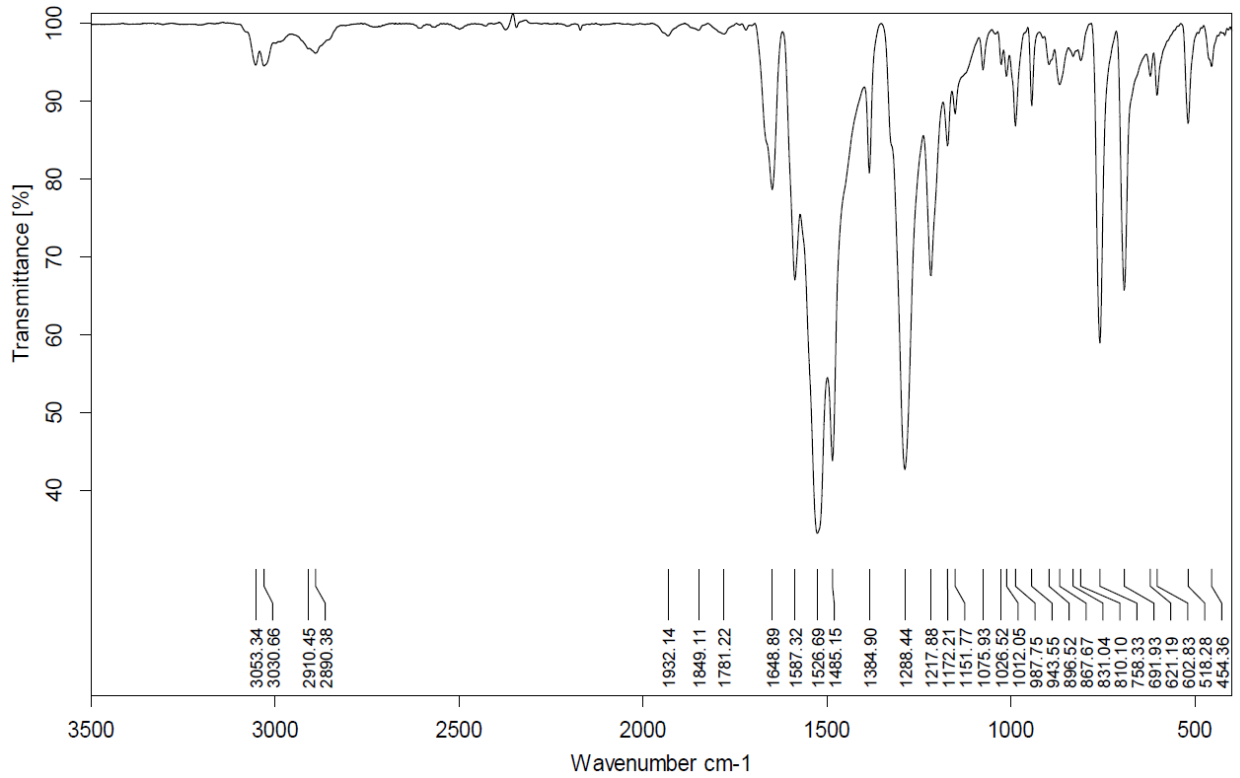

Figure S14. Infrared spectrum of Y{κ^2-(NPh)$_2$CH}$_3$ (KBr).

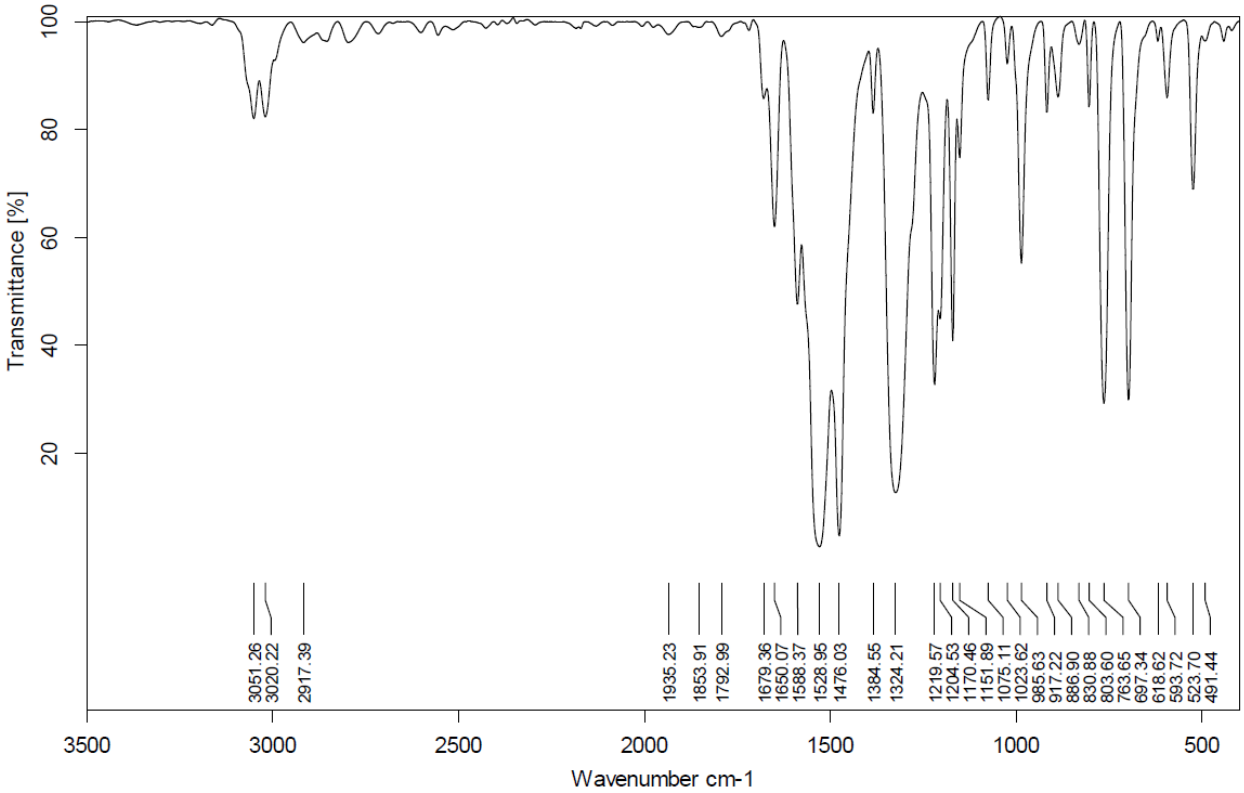

Figure S15. Infrared spectrum of La{κ^2-(NPh)$_2$CH}$_3$ (KBr).

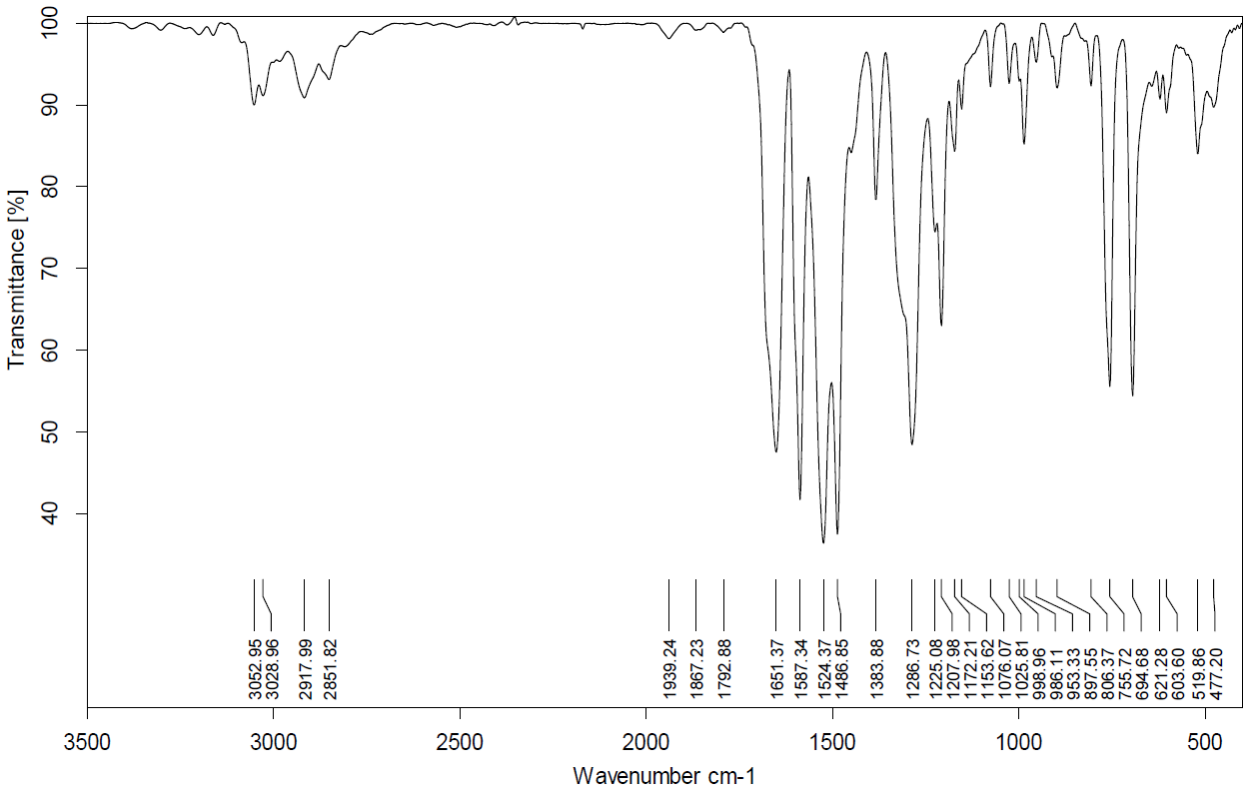

Figure S16. Infrared spectrum of Sc{κ^2-(NPh)$_2$CH}$_3$ (KBr).

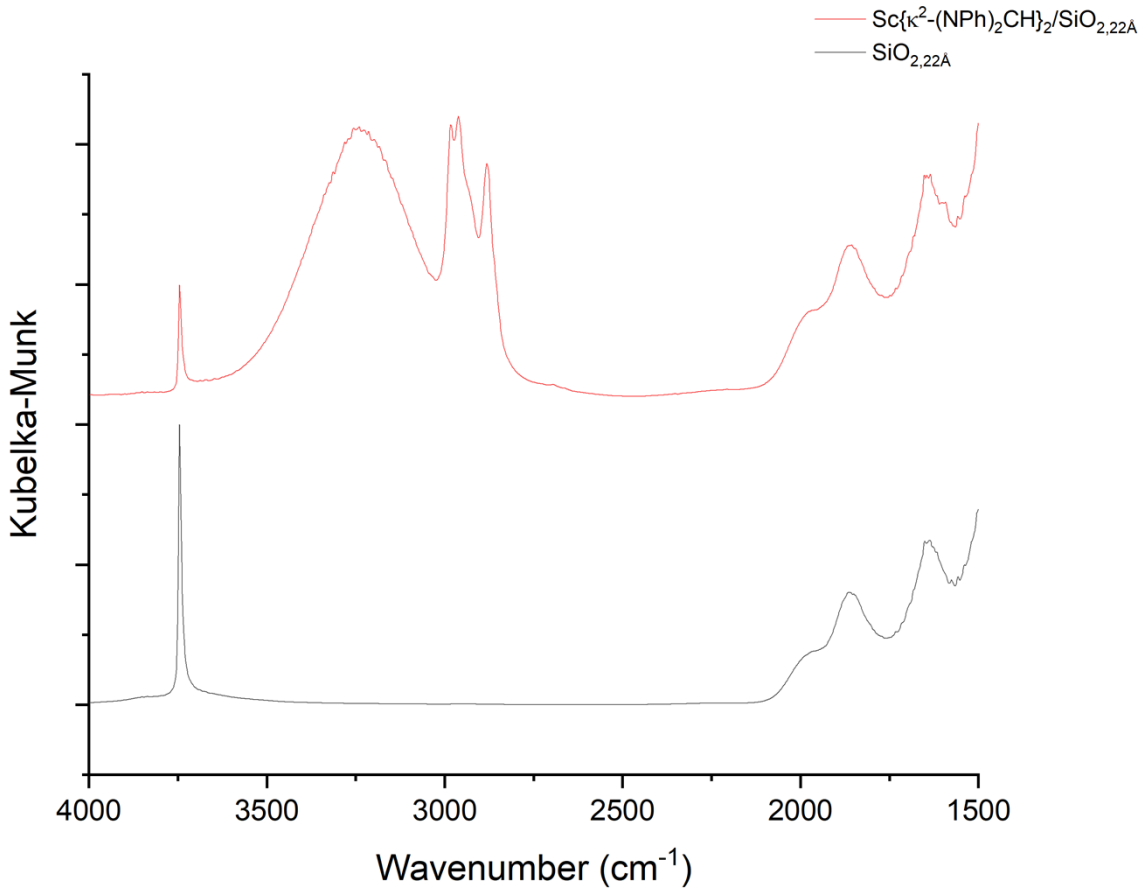

Figure S17. DRIFTS of $SiO_{2,22Å}$ and Sc{κ^2-(NPh)$_2$CH}$_2$/$SiO_{2,22Å}$.

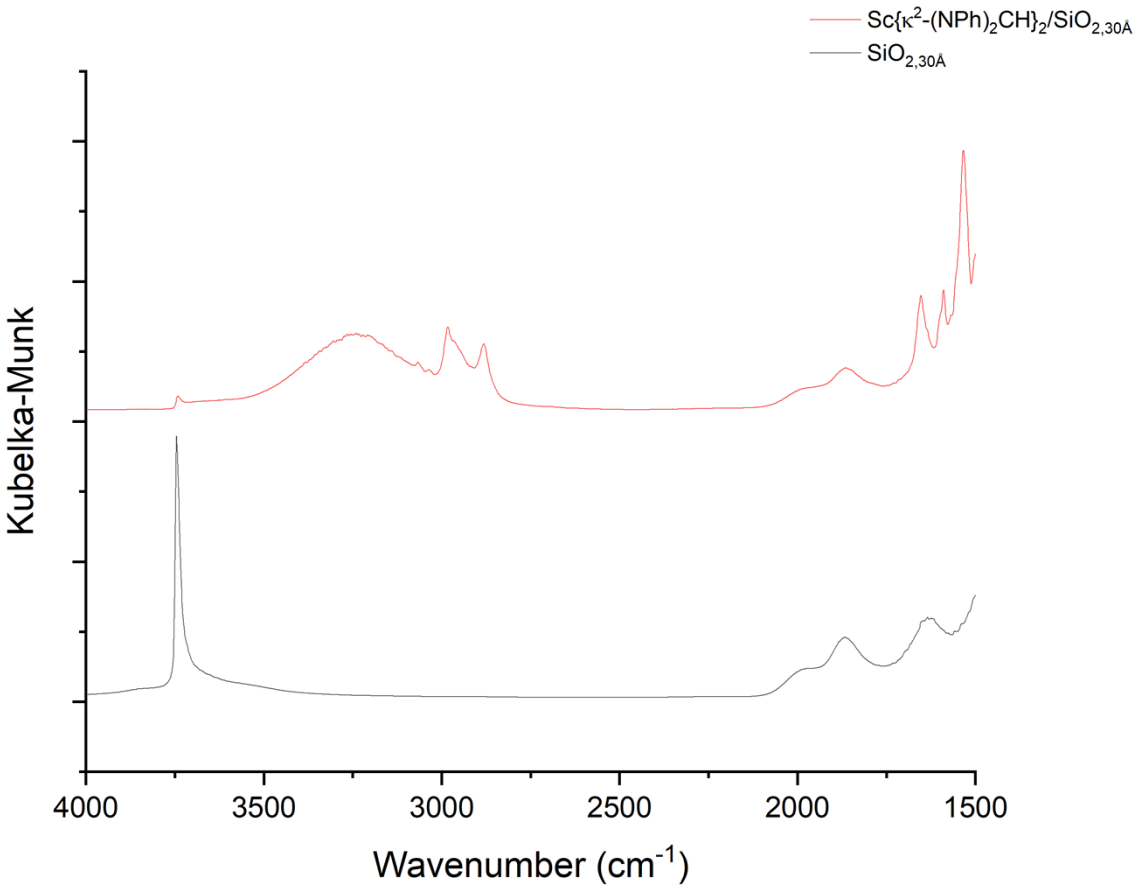

Figure S18. DRIFTS of $SiO_{2,30Å}$ and $Sc\{\kappa^2\text{-}(NPh)_2CH\}_2/SiO_{2,30Å}$.

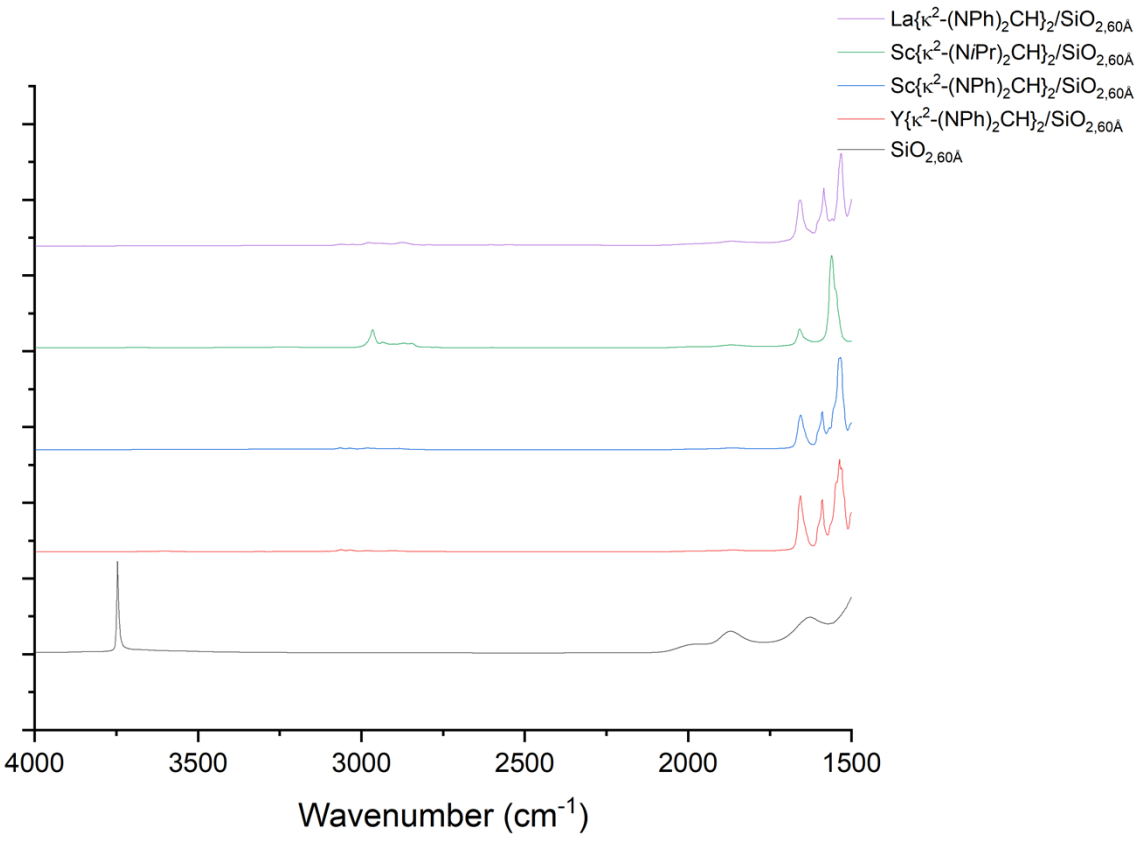

Figure S19. DRIFTS of $SiO_{2,60Å}$, $Y\{\kappa^2\text{-}(NPh)_2CH\}_2/SiO_{2,60Å}$, $Sc\{\kappa^2\text{-}(NPh)_2CH\}_2/SiO_{2,60Å}$, $Sc\{\kappa^2\text{-}(NiPr)_2CH\}_2/SiO_{2,60Å}$, and $La\{\kappa^2\text{-}(NPh)_2CH\}_2/SiO_{2,60Å}$.

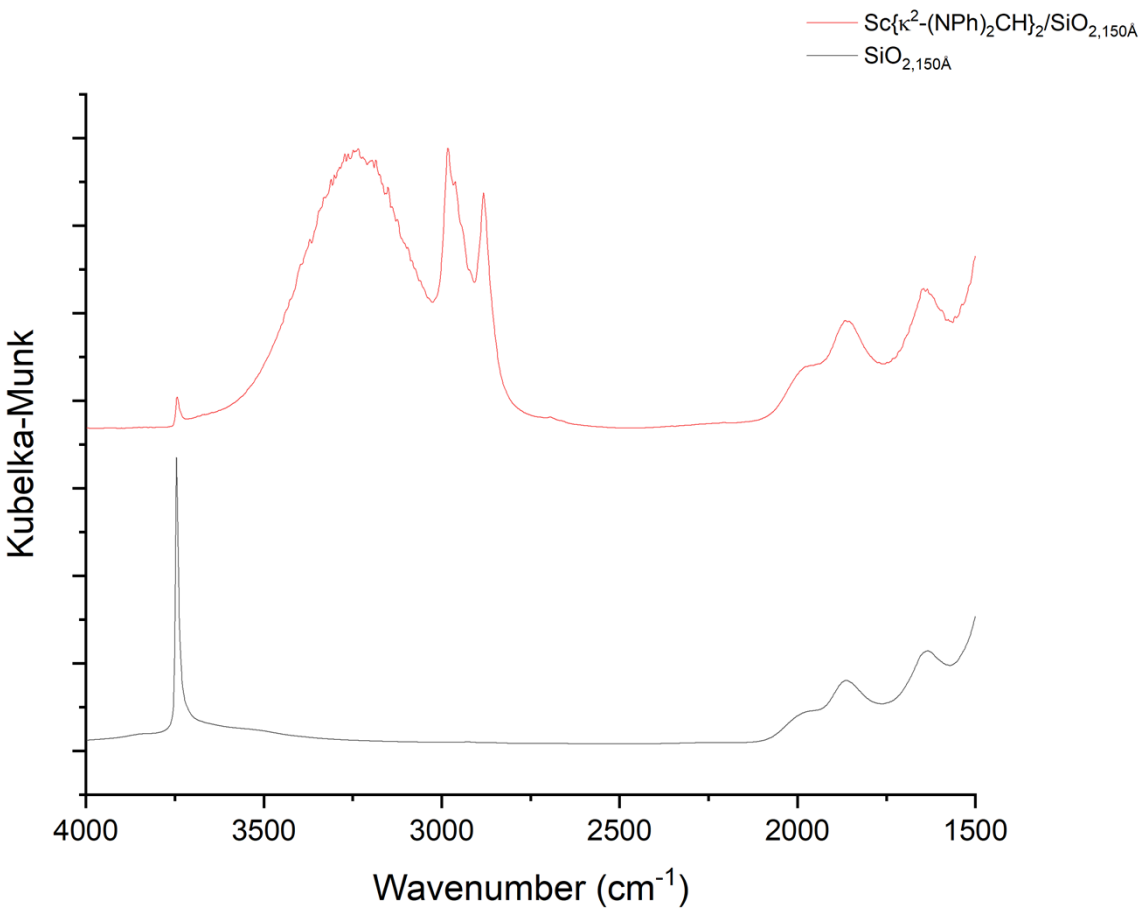

Figure S20. DRIFTS of $SiO_{2,150Å}$ and $Sc\{\kappa^2\text{-}(NPh)_2CH\}_2/SiO_{2,150Å}$.

3. DFT Calculations

3.1. Example ADF input file

The list of constraints and atomic coordinates are omitted for clarity.

```
#!/bin/sh

"$AMSBIN/ams" << eor

Task GeometryOptimization
Constraints
   [placeholder]
End
System
    Atoms
    [placeholder]
    End
End

Engine ADF
    Basis
        Type TZP
        Core None
        PerAtomType Symbol=Sc File=ZORA/TZ2P+/Sc
    End
```

```
    Save TAPE10
    XC
        Hybrid PBE
        Dispersion Grimme4
    End
    Relativity
        Level Spin-Orbit
    End
    Symmetry NOSYM
    NumericalQuality VeryGood
EndEngine
eor
```

3.2. Geometry optimized coordinates of Sc{κ²-(NPh)$_2$CH}$_2$/SiO$_2$

```
70
C29H31N4O4ScSi optimized with ADF in AMS.
 C       13.48138496761232      16.78676126217711      10.60468429496014
 H       11.13721324669378      15.87385684142458      12.46945349074984
 H       13.91854224292237      20.15905145038104      10.90910712551451
 N       15.04113659646595      17.46481565033228      16.29935609347080
 H       16.92877332971764      18.43557885111280      16.00499194109601
 H       12.91116285799560      11.41263586328272      16.06902330211137
 H       16.14234856417730      15.06914912438902      13.18867206436716
 H       11.80846652864611      12.65869676161256      16.72393901977540
 Sc      13.71376697808648      17.24673438140375      14.56005973695993
 C       14.14712203548459      17.76762965824577       8.49073068539501
 H       13.52476848708381      19.73770886424871      16.95520592475728
 H       15.00929478822638      14.19735303506831      12.10346312667041
 H        9.81290543377408      14.96103941842600      13.24749765729765
 H       17.25056016753526      17.47156003149151      17.92591381514087
 N       12.79478993438279      19.23933539937147      14.49871432200476
 C       12.31691070246747      12.30034727225807      15.81592078671244
 C       13.81336156828193      16.64711322379470       9.25900709362817
 C       14.15727686863427      19.02894664513301       9.09365211742674
 N       13.17057625804341      18.12813926765456      12.57773675638882
 H       14.44260273035152      19.90865609978450       8.51296903730770
 C       13.83899596035112      19.17604672639844      10.44256984682252
 H       14.40876048071817      17.65734829904465       7.43710616156284
 C       10.72689993743299      14.86787418481413      12.64324498072196
 C       13.47944083559836      18.05516692435672      11.21708761207299
 H       13.21860321061445      15.91538845744823      11.20640130738989
 C       12.78071058556354      19.25764854693757      13.16612764237774
 H       13.80783220849769      15.65439808270440       8.80367762151331
 N       15.87179054239730      17.85469486573077      14.24614026443859
 H       12.48041503126133      20.15230663505781      12.59450072962543
 O       11.67051832943588      14.00372689165987      13.30419777926160
 H       11.56656374439804      12.03008146326748      15.05836746191749
 C       15.24291381737301      14.44328056111867      13.14929041891784
 O       14.16007494794319      15.19400916883419      13.72870174748310
 H       10.47758349901193      14.41006301182204      11.67691978520941
 Si      12.73118527324095      14.58091803527058      14.42311040872172
 O       12.29425208708063      15.97119438966152      15.11888638468040
 O       13.22079540792112      13.30074731756619      15.32050993147919
 H       15.40494837753957      13.52093246218170      13.72262299483539
 C       16.03939319804608      17.95761549817708      15.55936122337590
 H       17.20287452872359      20.20532751919788      14.62733685500578
 C       12.26870835689127      20.27115172436489      15.28286117074186
 C       11.25869882202841      21.14234197270367      14.82946543266803
 C       10.77843012365491      22.15464468639339      15.66012630685224
 C       11.27477187222481      22.30722728659727      16.95803648843286
 C       12.25963381023324      21.42836119951895      17.42114970630532
 C       12.75329547320612      20.42081790514493      16.59595170653752
 H       10.82522775134784      21.00737777161059      13.83683024523748
```

H	9.99237998844477	22.81894882024298	15.29468007382873
H	10.88720083291513	23.09442559634797	17.60680311179208
H	12.64877109341492	21.52729878162683	18.43655584306803
C	16.67824018444037	18.54367691740417	13.33272276299048
C	16.79777494697885	18.02790706463815	12.02886149640277
C	17.57342231718263	18.68128097551808	11.07484442828825
C	18.24722061236234	19.86345185033754	11.39807030210124
C	18.12105772010783	20.39274657394433	12.68595433905225
C	17.33655872084429	19.75040825011745	13.64401866439975
H	16.26116795595771	17.11381698708145	11.77237982309699
H	17.64369157308525	18.26736367273826	10.06710211213785
H	18.85130784518669	20.37753248410873	10.64854258323650
H	18.62051835376809	21.32947559226223	12.94273637828396
C	15.09087923134177	17.36388258487601	17.69233996674933
C	13.87356537319396	17.19822666259163	18.38155757609462
C	13.85262808597845	17.10448412249988	19.77093567317540
C	15.04148101789381	17.16821370354077	20.50533558007920
C	16.25533378941726	17.31127922016611	19.82684935171546
C	16.28821251541980	17.39999575824449	18.43536432682065
H	12.94699845779267	17.14035719956896	17.80644264433283
H	12.89763909911142	16.97957373494133	20.28539017502046
H	15.02397761375724	17.09315695475397	21.59383636721335
H	17.19297027509141	17.33908639218193	20.38622639659691

4. Supplementary References

1 M. Bak and N. C. Nielsen, REPULSION, A Novel Approach to Efficient Powder Averaging in Solid-State NMR, *J. Magn. Reson.*, 1997, **125**, 132–139.

2 M. H. Levitt, *Spin Dynamics: Basics of Nuclear Magnetic Resonance*, Wiley, 2nd edn., 2008.